Model Predictive Control of the Interleaved DC-DC Boost Converter with Coupled Inductors

Petros Karamanakos[*], Tobias Geyer[†], Stefanos Manias[*]
[*] National Technical University of Athens (NTUA)
Iroon Polytechniou 9
15780 Zografou, Greece
Phone: +30 210-772.22.33
Fax: +30 210-772.35.93
Email: petkar@central.ntua.gr, manias@central.ntua.gr
URL: http://www.ntua.gr
[†] ABB Corporate Research
Segelhofstrasse 1K
5405 Baden-Dättwil, Switzerland
Phone: +41 058-586.86.88
Fax: +41 058-586.40.06
Email: t.geyer@ieee.org
URL: http://www.abb.com

Keywords

<<Optimal control>>, <<Non-linear control>>, <<Converter control>>.

Abstract

This paper proposes a model predictive control (MPC) scheme for the interleaved dc-dc boost converter with coupled inductors. The main control objectives are the regulation of the output voltage to its reference value, despite changes in the input voltage and the load, and the equal sharing of the load current by the two circuit inductors. An inner control loop, using MPC, regulates the input current to its reference that is provided by the outer loop, which is based on a load observer. Simulation results are provided to highlight the performance of the proposed control scheme.

Introduction

Nowadays, demanding high power applications that require high current are in widespread use. However, the conventional boost converter is not suitable for high step-up dc-dc conversion because of its high duty cycle, hard switching operation and output diode reverse-recovery problem. Despite the fact that dc-dc power conversion is a mature technology used in numerous applications [1], new topologies are required that allow current sharing, which is highly demanded in order to avoid inductor saturation, degraded converter performance, and uneven thermal stresses. In [2], a novel dc-dc boost converter is proposed with two coupled inductors, which exploits the benefits of continuous (CCM) and discontinuous (DCM) conduction modes: the converter operates in CCM, with respect to the input current, resulting in a reduced input current ripple. On the other hand, zero boost-rectifier reverse-recovery losses are achieved, when considering the currents of the individual converter legs, since these legs operate in DCM.

When designing controllers for boost converters, it is common practice to use an outer voltage control loop and an inner current loop; the inner control loop drives the input current to a desired reference, which is derived by the outer loop that regulates the output voltage to its reference value. If the control loops are properly designed then the voltage regulation is achieved, while the controller rejects all disturbances. Furthermore, a controller applied to the interleaved converter should aim to distribute equally the input current between the two inductors.

In this paper, the current regulation problem is solved by adopting model predictive control (MPC) [3, 4]. An objective function wherein the user has the flexibility to weigh competing interests such as

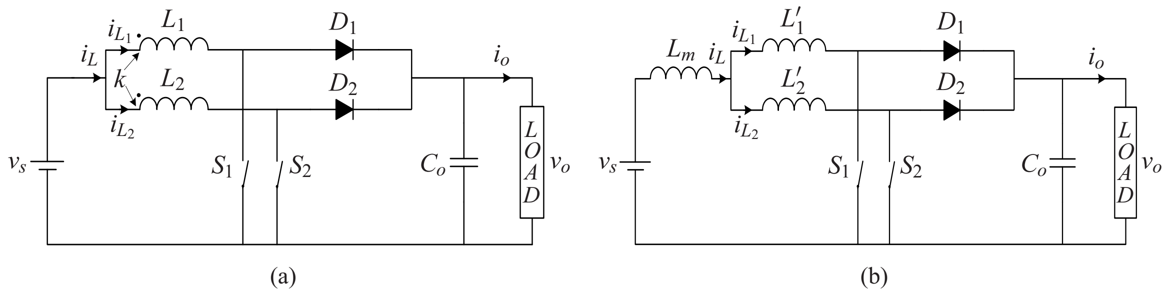

Figure 1: (a) Topology of the interleaved dc-dc boost converter with coupled inductors and (b) the equivalent circuit.

voltage and/or current tracking, switching frequency, etc, is formulated based on the mathematical model of the converter, and it is minimized over a prediction horizon of finite length in time. Furthermore, hysteresis bounds used as soft constraints [5–9], and switching constraints, imposed as hard constraints, are implemented so as to achieve the favorable performance of the converter examined[1]. The underlying optimization problem is solved in real-time. The sequence of control inputs that results in the best predicted performance of the plant is considered to be *optimal*, and the first element of this sequence is applied to the converter. In order to provide feedback, the so-called *receding horizon strategy* is employed: the remaining elements of the optimal sequence are discarded, the horizon is shifted by one sampling interval, and the procedure is repeated at the next sampling instant, using new measurements. Finally the reference of the current is derived from an outer loop using a power balance expression, while a load observer is employed for estimating the load current. This outer loop serves solving the voltage regulation problem.

The proposed approach has several benefits, such as inherent robustness and very fast transient response. Furthermore, the tuning is simple due to the straightforward controller design process. However, the computational burden can become high as the prediction horizon increases; this makes the real-time implementation of the controller challenging. This problem is solved with the proposed method: firstly, the hard constraints reduce the number of the feasible paths, i.e. the switching paths that meet the switching constraints; the respective number of calculations decreases. Most importantly, the control problem is treated as a *current* regulation problem [10], not a voltage regulation problem [11]. This implies that only a relatively short horizon is required, since the current exhibits minimum-phase behavior with respect to the control input [1].

Mathematical Model

The topology of the interleaved dc-dc boost converter with coupled inductors is shown in Fig. 1(a). It consists of the two coupled inductors L_1 and L_2, whose windings have the same orientation. As shown in [2], the equivalent circuit of the coupled inductors can be represented by three uncoupled inductors (see Fig. 1(b)), where L_1' and L_2' are the leakage inductances of the two inductors, and L_m is the mutual inductance, given by

$$L_1' = L_1 - L_m \tag{1a}$$
$$L_2' = L_2 - L_m \tag{1b}$$
$$L_m = k\sqrt{L_1 L_2}\,, \tag{1c}$$

where k is the coupling coefficient.

The possible switching combinations of the converter are: $S_1S_2 = 10$, $S_1S_2 = 00$ and $S_1S_2 = 01$, where "0" denotes the *off* state and "1" the *on* state of the power semiconductors. It is not allowed to turn both switches *on* simultaneously to facilitate current sharing between the inductors (first switching constraint). When switching from $S_1S_2 = 10$ to the complementary state $S_1S_2 = 01$, or vice versa, switching via $S_1S_2 = 00$ is a mandatory intermediate step (second switching constraint).

Considering the inductor currents $i_{L_1}(t)$, $i_{L_2}(t)$ and the output voltage $v_o(t)$ as the independent states of the converter, the state vector is defined as $x(t) = [i_{L_1}(t)\ i_{L_2}(t)\ v_o(t)]^T$. The system is described by the following affine equations, depending on the switch positions and the operating modes of the individual

[1]Soft constraints are these control related constraints that can be violated, but the degree of violation is weighted by a constant, while hard constraints are these constraints that cannot be violated under any circumstances.

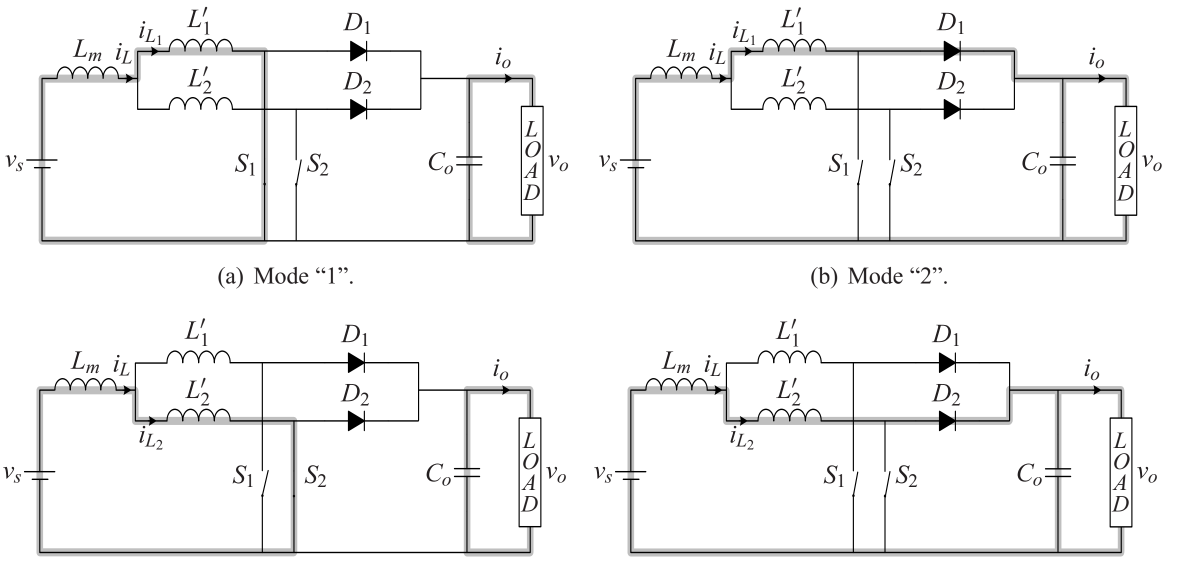

(a) Mode "1". (b) Mode "2".

(c) Mode "3". (d) Mode "4".

Figure 2: Basic operating modes and current paths of the interleaved dc-dc boost converter with coupled inductors.

converter legs (see Fig. 2)

$$\frac{dx(t)}{dt} = \begin{cases} B_1 w(t) & S_1 = 1 \ \& \ (S_2 = 0 \ \& \ i_{L_2}(t) = 0) & \text{Mode "1"} \\ A_1 x(t) + B_1 w(t) & S_1 = 0 \ \& \ (S_2 = 0 \ \& \ i_{L_2}(t) = 0) & \text{Mode "2"} \\ B_2 w(t) & S_2 = 1 \ \& \ (S_1 = 0 \ \& \ i_{L_1}(t) = 0) & \text{Mode "3"} \\ A_2 x(t) + B_2 w(t) & S_2 = 0 \ \& \ (S_1 = 0 \ \& \ i_{L_1}(t) = 0) & \text{Mode "4"} \end{cases}, \tag{2}$$

where $w(t) = [v_s(t) \ i_o(t)]^T$ is the vector of the disturbances, which are the input voltage $v_s(t)$ and the load current $i_o(t)$. The matrices A_1, A_2, B_1 and B_2 are given by

$$A_1 = \begin{bmatrix} 0 & 0 & -\frac{1}{L_1} \\ 0 & 0 & 0 \\ \frac{1}{C_o} & 0 & 0 \end{bmatrix}, \ A_2 = \begin{bmatrix} 0 & 0 & 0 \\ 0 & 0 & -\frac{1}{L_2} \\ \frac{1}{C_o} & 0 & 0 \end{bmatrix}, \ B_1 = \begin{bmatrix} \frac{1}{L_1} & 0 \\ 0 & 0 \\ 0 & -\frac{1}{C_o} \end{bmatrix}, \text{ and } B_2 = \begin{bmatrix} 0 & 0 \\ \frac{1}{L_2} & 0 \\ 0 & -\frac{1}{C_o} \end{bmatrix}.$$

The switches S_1 and S_2 are modeled using the binary variables $u_1, u_2 \in \{0,1\}$. Due to the fact that the individual converter legs operate in DCM, two current paths correspond to the same switching combination $S_1S_2 = 00$ (modes "2" and "4" shown in Figs. 2(b) and 2(d), respectively). Furthermore, two additional auxiliary binary variables $d_{\text{aux}_1}, d_{\text{aux}_2} \in \{0,1\}$ are introduced to model the switching state of the diodes [12]. When $d_{\text{aux}_n} = 1$, with $n \in \{1,2\}$, the nth leg of the converter operates in CCM ($S_n = 1$ or $S_n = 0$ and $i_{L_n}(t) > 0$); when $d_{\text{aux}_n} = 0$ the nth leg operates in DCM ($S_n = 0$ and $i_{L_n}(t) \leq 0$), see Fig. 3.

The MPC controller is based on a discrete-time state-space model of the converter; this is derived by combining (2) into one continuous-time non-linear expression and discretizing it using the forward Euler approximation approach. This yields

$$x(k+1) = \big(\mathbb{I} + \Gamma_1 T_s + \Gamma_2(u) T_s\big) x(k) + \Delta T_s w(k) \tag{3}$$

where $u = \{u_1, \ u_2\}$ is the input vector, with u_1 and u_2 referring to the switching state of S_1 and S_2 respectively, and $\Gamma_1 = d_{\text{aux}_1} A_1 + d_{\text{aux}_2} A_2, \Gamma_2 = -u_1 A_1 - u_2 A_2$ and $\Delta = d_{\text{aux}_1} B_1 + d_{\text{aux}_2} B_2$. Furthermore, $\mathbb{I}$ denotes the identity matrix, and T_s is the sampling interval. Finally, by introducing the matrix

$$C = \begin{bmatrix} 0 & 0 & 1 \end{bmatrix},$$

the output of the system is defined as

$$y(k) = Cx(k). \tag{4}$$

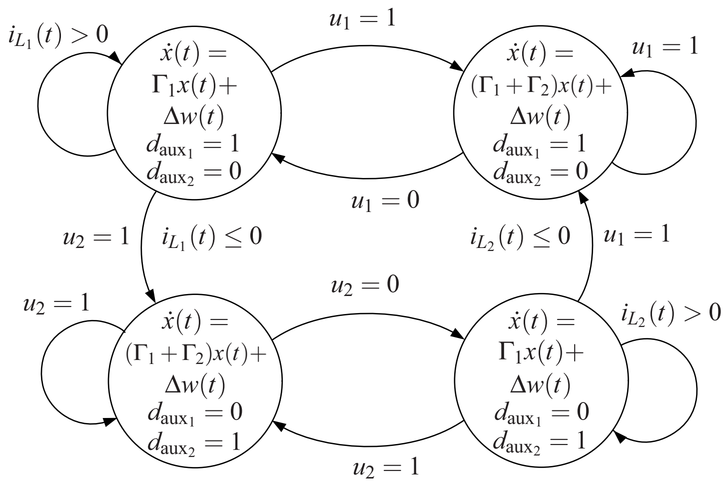

Figure 3: Dc-dc interleaved converter with coupled inductors presented as an automaton driven by conditions.

Model Predictive Control

The control objective of the interleaved converter with coupled inductors is twofold. First, an output voltage equal to a predefined value is to be achieved, despite measurable changes in the input voltage and unmeasurable variations in the load. The second objective is to achieve equal current sharing among the parallel legs of the converter. Both objectives are of equal importance. The structure of the proposed control scheme is illustrated in Fig. 4. It consists of an inner current control loop and an outer voltage regulation loop.

Outer Voltage Control Loop

Regarding the voltage regulation problem, a power balance expression is used and a load observer is employed to estimate the load current. Specifically a second order Luenberger observer is designed [8] in order to decouple the controller design from the load characteristics [13]. Using an observer to estimate—rather than measure—the load current also contributes to hardware-related cost reduction. The observer estimates the value of the load current, $\hat{i}_o$, according to

$$\hat{x}_e(k+1) = F\hat{x}_e(k) + G(u) + H\overline{y}_e(k) \tag{5a}$$

$$\hat{y}_e(k) = M\hat{x}_e(k) \tag{5b}$$

where $\hat{x}_e = [\hat{i}_o \ \hat{v}_o]^T$ is the observed state vector, consisting of the load current $\hat{i}_o$ and output voltage $\hat{v}_o$. The term $\overline{y}_e$ represents the error between the measured and the observed value of the output variable of the system y_e, which is the output voltage, i.e. $y_e = v_o$, and $H = [h_1 \ h_2]^T$ describes the constant observer gain. The matrices F, G and M are

$$F = \begin{bmatrix} 1 & 0 \\ -\frac{T_s}{C_o} & 1 \end{bmatrix}, \ G = T_s \begin{bmatrix} 0 & 0 \\ \frac{i_{L_1}(1-u_1)d_{\text{aux}_1}}{C_o} & \frac{i_{L_2}(1-u_2)d_{\text{aux}_2}}{C_o} \end{bmatrix}, \text{ and } M = \begin{bmatrix} 0 & 1 \end{bmatrix}.$$

Hence, the controller is based on the estimated value of the load current $\hat{i}_o$, rather than the measured one i_o.

In order to calculate the current reference of the inner control loop, the power balance of the converter, i.e. $P_{in} = P_{out}$, is taken into account. It assumes that the power switches and the inductors are ideal, in a first approximation. Using small-ripple approximation [1], i.e. $v_s \approx V_s$, $v_{o,\text{ref}} \approx V_{o,\text{ref}}$ and $\hat{i}_o \approx \hat{I}_o$ the reference current is derived:

$$I_{L,\text{ref}} = \frac{V_{o,\text{ref}}\hat{I}_o}{V_s}. \tag{6}$$

Inner Current Control Loop

The inner controller is designed in the MPC framework, manipulating the switches S_1 and S_2. An objective function is formulated over a finite horizon, and hard and/or soft constraints are imposed.

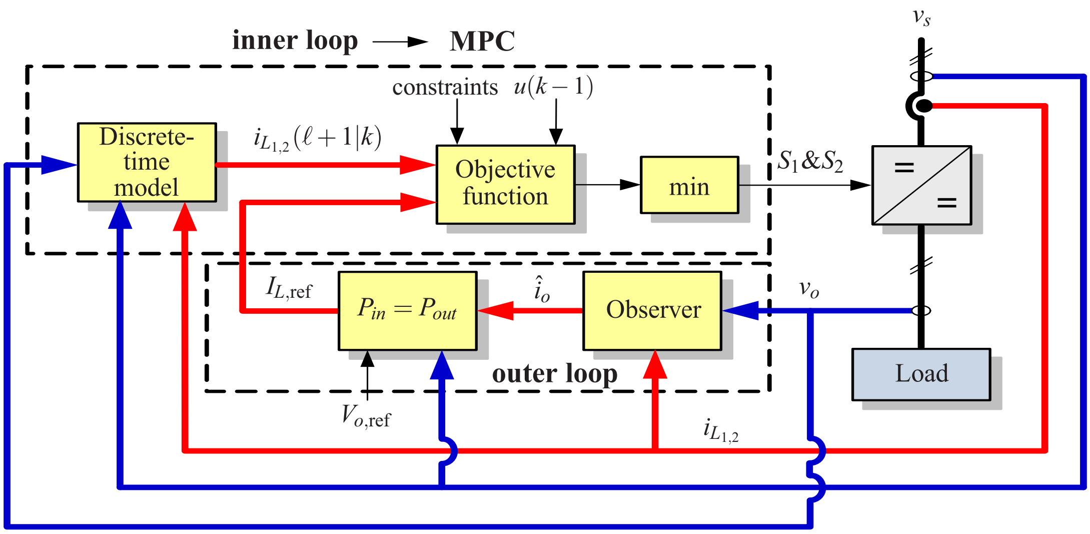

Figure 4: Block diagram of the proposed model predictive control (MPC) scheme.

At each sampling instant, the objective function is minimized subject to the constraints and the converter dynamics over the optimization variable, i.e. the sequence of switching states over a finite horizon $U(k) = [u(k)\ u(k+1) \ldots u(k+N-1)]^T$. The first value $u^*(k)$ of the derived optimal sequence U^* is applied to the converter, and the procedure is repeated at the next sampling instant based on the receding horizon strategy already explained.

In the following, the constraints that are imposed on the converter are introduced. Apart from the switching constraints mentioned in the previous section, hysteresis bounds are employed; these are soft constraints. They penalize the deviation of the input current, i.e. the sum of the inductor currents $i_L(k) = i_{L_1}(k) + i_{L_2}(k)$, from its reference. The weighted amount of the bound violation is described by the slack variable $e(k)$ [14] given by

$$e(k) = \begin{cases} p_a\ (i_L(k) - I_{L,\max}) & \text{if } i_L \geq I_{L,\max} \\ p_a\ (I_{L,\min} - i_L(k)) & \text{if } i_L \leq I_{L,\min} \\ p_b\ |i_L(k) - I_{L,\mathrm{ref}}| & \text{otherwise} \end{cases} \tag{7}$$

where $p_a,\ p_b \in \mathbb{R}^+$ are the weighting factors of the soft constraints, while the terms $I_{L,\max}$ and $I_{L,\min}$ are specified as a percentage of the reference current $I_{L,\mathrm{ref}}$.

An objective function is chosen that penalizes the evolution of the error over the finite horizon N using the 1-norm (sum of absolute values). In addition, the switching transitions are penalized and weighted by the factor $p_c \in \mathbb{R}^+$ in order to decrease the switching frequency and to avoid excessive switching:

$$J(k) = \sum_{\ell=k}^{k+N-1} \Big(||e(\ell+1|k)||_1 + p_c||u(\ell) - u(\ell-1)||_1 \Big). \tag{8}$$

Finally the control input, i.e. the optimal sequence of switching states, is obtained by minimizing (8), subject to the discrete-time state-space model of the converter, as well as the current and the switching constraints.

$$\begin{aligned} & U^*(k) = \arg\min J(k) \\ & \text{subject to eq. (3), (4), (7) and switching constraints} \end{aligned} \tag{9}$$

Performance Evaluation

Using the equivalent circuit of the converter, the performance of the proposed control scheme is investigated. Concerning the converter parameters, the coupled inductors are $L_1 = L_2 = 0.91$ mH, the coupling coefficient is $k = 0.93$, and the filter capacitance is $C_o = 220\,\mu$F. The input voltage is $v_s = 20$ V, the load resistance is $R = 75\,\Omega$, and the reference of the output voltage is set to $V_{o,\mathrm{ref}} = 45$ V. Finally, the sampling interval is $T_s = 20\,\mu$s. With regards to the objective function, the factor p_a is chosen to be $p_a \gg p_b$ in order to penalize more heavily the violation of the current bounds, while p_c sets the trade-off between

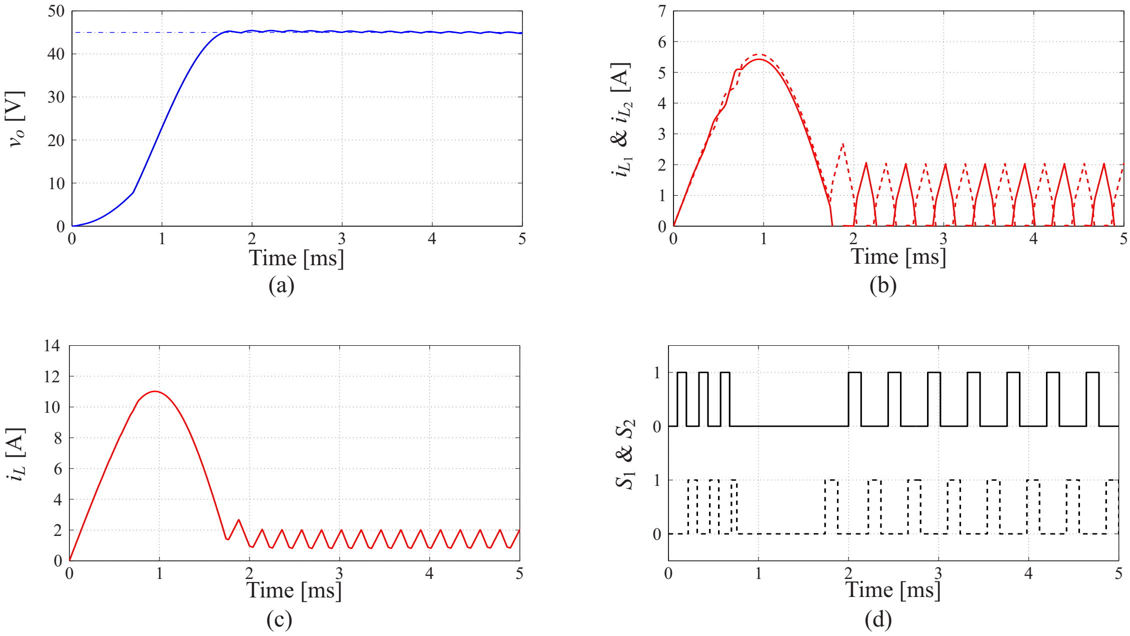

Figure 5: Simulation results for nominal start-up with MPC: (a) Output voltage (solid line) and reference voltage (dash-dotted line), (b) inductor currents i_{L_1} (solid line) and i_{L_2} (dashed line), (c) input current, and (d) the corresponding switching states of S_1 (solid line) and S_2 (dashed line).

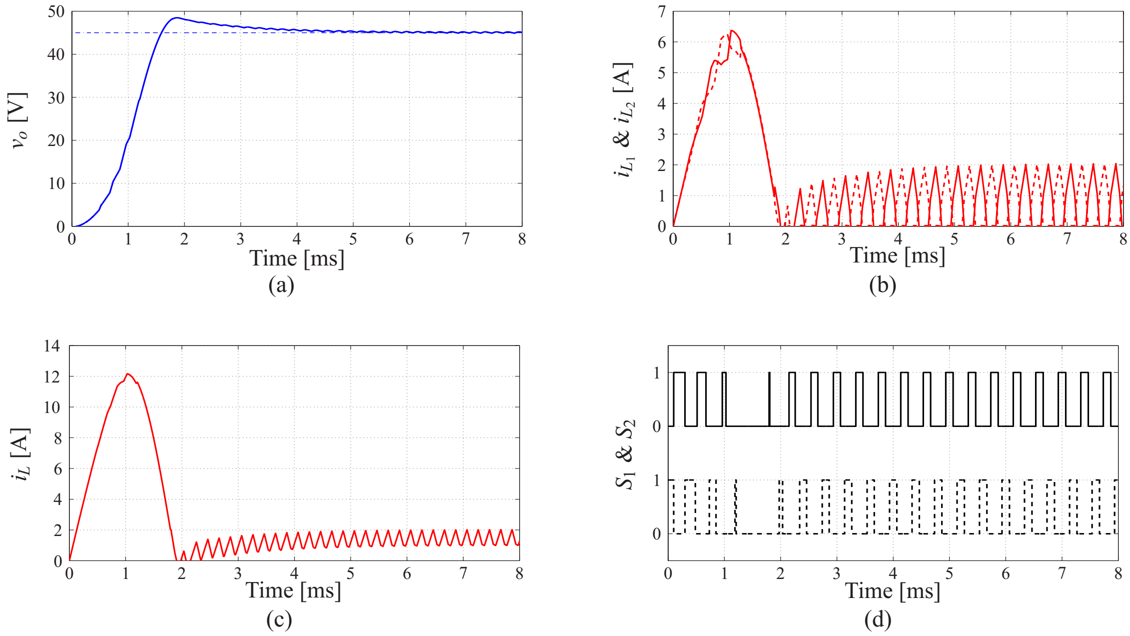

Figure 6: Simulation results for nominal start-up with a PI controller: (a) Output voltage (solid line) and reference voltage (dash-dotted line), (b) inductor currents i_{L_1} (solid line) and i_{L_2} (dashed line), (c) input current, and (d) the corresponding switching states of S_1 (solid line) and S_2 (dashed line).

the inductor current error and the switching frequency. Thus, the weighting factors heuristically chosen are $p_a = 5$, $p_b = 0.01$ and $p_c = 0.1$. The current bounds are $I_{L,\max} = 1.1 I_{L,\text{ref}}$, and $I_{L,\min} = 0.9 I_{L,\text{ref}}$. The prediction horizon is $N = 5$.

The controller enumerates all the switching sequences that meet the switching constraints within the horizon to predict the evolution of the error $e(k)$. The switching sequence that minimizes the objective function (8) is chosen, and the first element of this sequence, the switching states at time-step k, is applied to the converter.

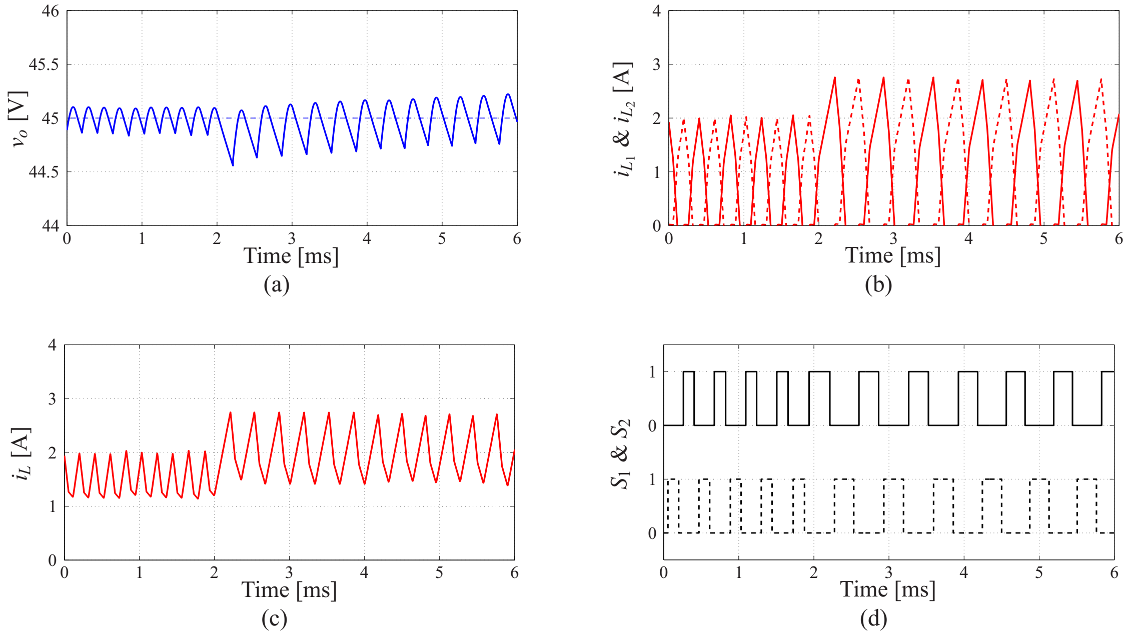

Figure 7: Simulation results for a step-down change in the input voltage with MPC: (a) Output voltage (solid line) and reference voltage (dash-dotted line), (b) inductor currents i_{L_1} (solid line) and i_{L_2} (dashed line), (c) input current, and (d) the corresponding switching states of S_1 (solid line) and S_2 (dashed line).

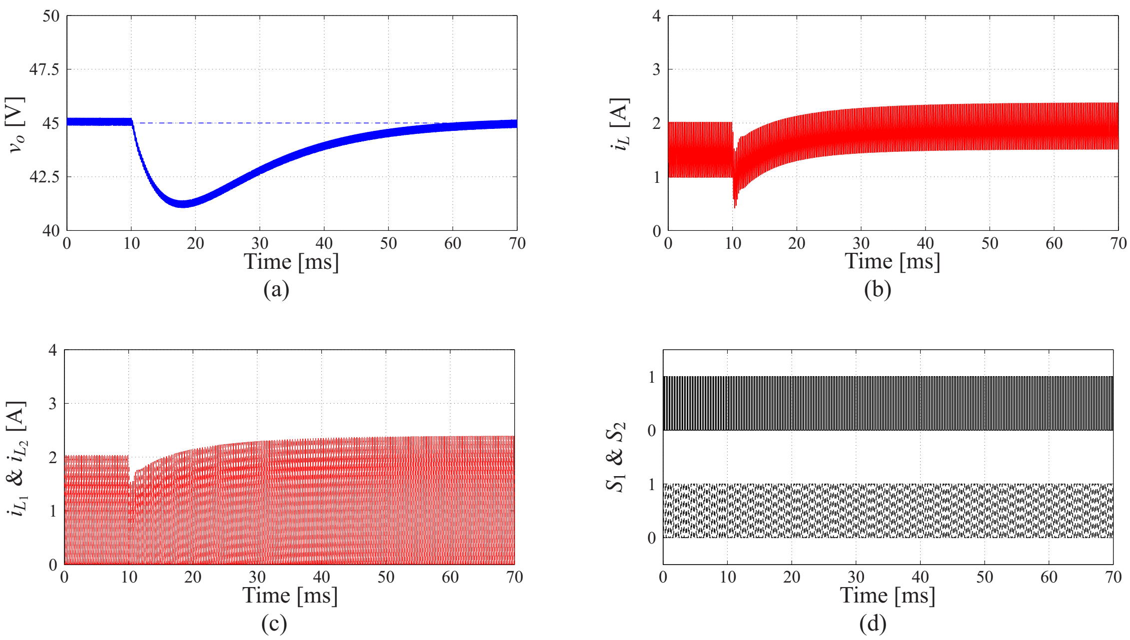

Figure 8: Simulation results for a step-down change in the input voltage with a PI controller: (a) Output voltage (solid line) and reference voltage (dash-dotted line), (b) inductor currents i_{L_1} (solid line) and i_{L_2} (dashed line), (c) input current, and (d) the corresponding switching states of S_1 (solid line) and S_2 (dashed line).

Nominal Start-Up

The first case to be examined is that of the nominal start-up. As can be seen in Fig. 5, the inductor currents increase until the capacitor is charged to the desired voltage level. The high transient current observed in Fig. 5(c) is required to achieve a very fast voltage response. The output voltage (Fig. 5(a)) reaches its reference value in about $t \approx 2\,\text{ms}$, with no overshoot. Once the transient phenomenon has occurred, the inductor currents (Fig. 5(b)) reach their nominal values and the output voltage remains constant at the desired level.

For comparison purposes, a conventional proportional-integral (PI) controller has been implemented (the

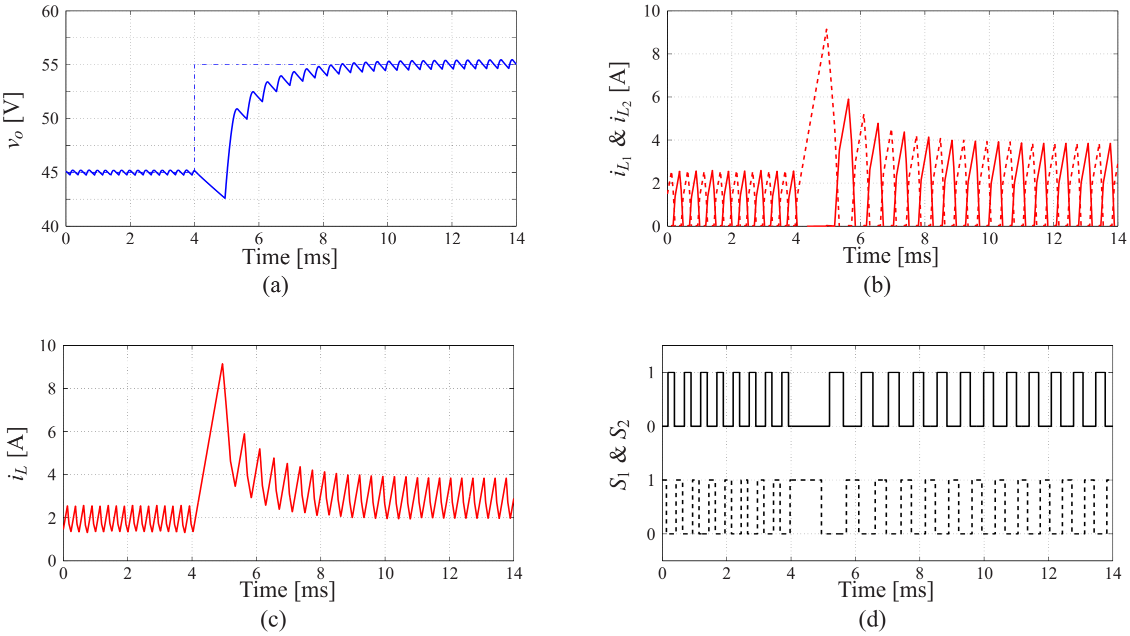

Figure 9: Simulation results for a step-up change in the output voltage reference with MPC: (a) Output voltage (solid line) and reference voltage (dash-dotted line), (b) inductor currents i_{L_1} (solid line) and i_{L_2} (dashed line), (c) input current, and (d) the corresponding switching states of S_1 (solid line) and S_2 (dashed line).

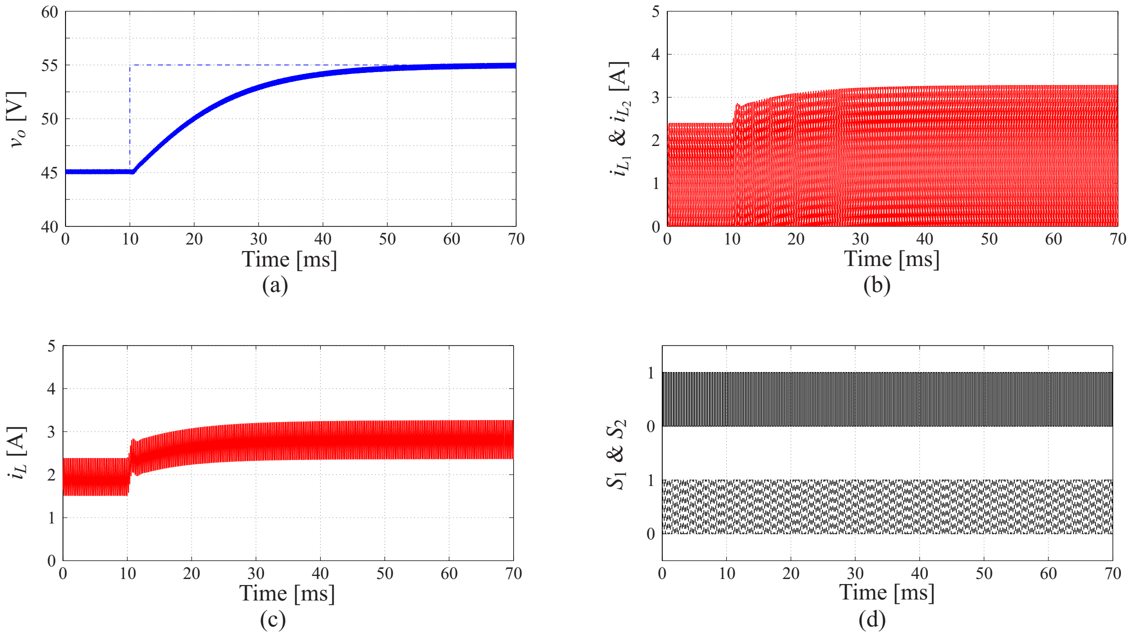

Figure 10: Simulation results for a step-up change in the output voltage reference with a PI controller: (a) Output voltage (solid line) and reference voltage (dash-dotted line), (b) inductor currents i_{L_1} (solid line) and i_{L_2} (dashed line), (c) input current, and (d) the corresponding switching states of S_1 (solid line) and S_2 (dashed line).

outer loop is the same). The respective voltage and current waveforms are shown in Fig 6. An overshoot of around 5% is observed in the output voltage (Fig 6(a)), resulting in a higher settling time compared to MPC, i.e. about $t \approx 5.5\,\text{ms}$.

Step Change in the Input Voltage

Operating at the previously attained operating point, the input voltage is changed in a step-wise manner. In Fig. 7 the closed-loop performance of the converter is depicted. At time $t = 2\,\text{ms}$ the input voltage is

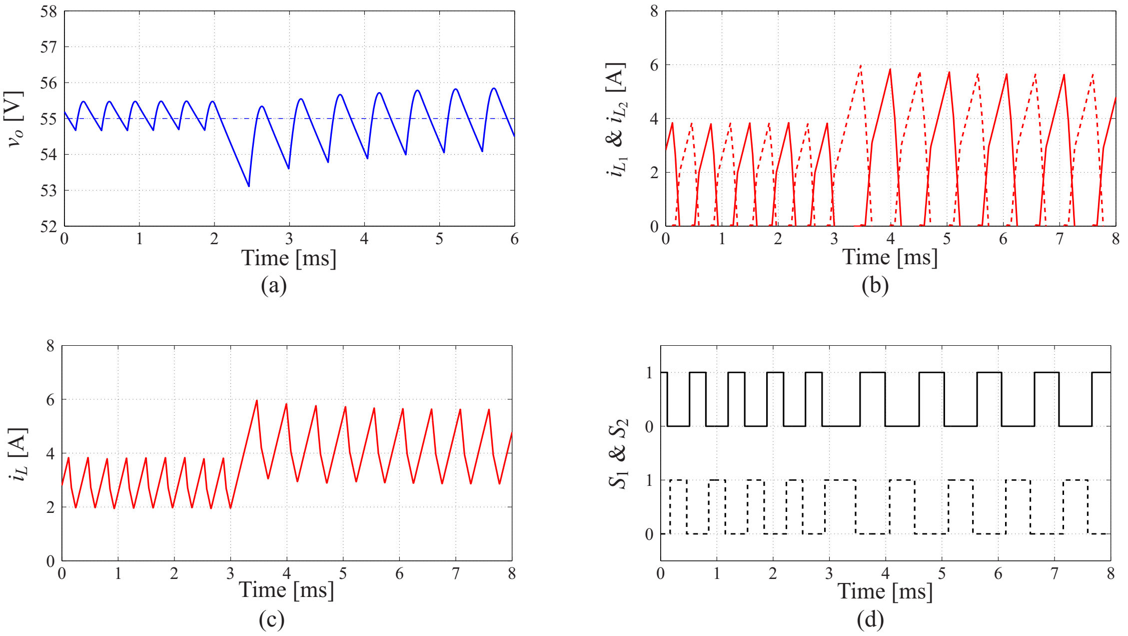

Figure 11: Simulation results for a step-down change in the load with MPC: (a) Output voltage (solid line) and reference voltage (dash-dotted line), (b) inductor currents i_{L_1} (solid line) and i_{L_2} (dashed line), (c) input current, and (d) the corresponding switching states of S_1 (solid line) and S_2 (dashed line).

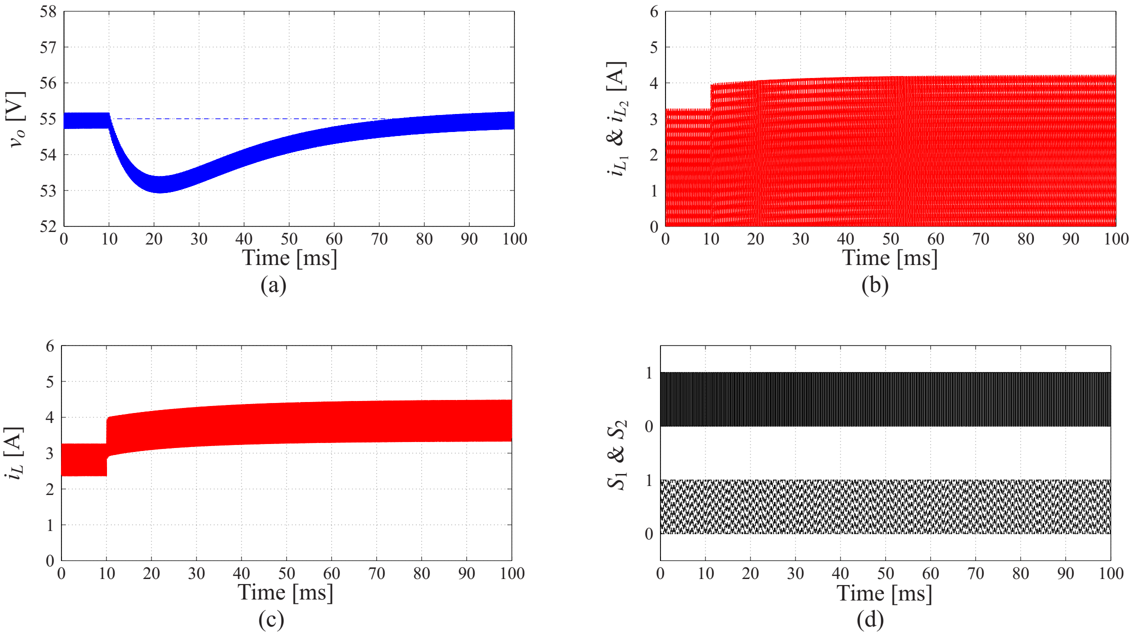

Figure 12: Simulation results for a step-down change in the load with a PI controller: (a) Output voltage (solid line) and reference voltage (dash-dotted line), (b) inductor currents i_{L_1} (solid line) and i_{L_2} (dashed line), (c) input current, and (d) the corresponding switching states of S_1 (solid line) and S_2 (dashed line).

decreased from $v_s = 20\,\text{V}$ to $v_s = 15\,\text{V}$. The inductor current instantaneously increases to its new nominal value (Fig. 7(c)), while the output voltage remains practically unaffected (Fig. 7(a)), with no significant undershoot observed. As can be seen the controller settles very quickly at the new steady-state operating point.

In Fig. 8 the response of the system when controlled by a PI controller is shown. Since controllers of this type are usually tuned to achieve optimal performance only over a narrow operating range, outside this range the performance is significantly deteriorated. This can be clearly seen in Fig. 8(a), where the output voltage after an undershoot reaches its reference value in about $t \approx 50\,\text{ms}$.

Step Change in the Output Reference Voltage

Next, a step-up change in the reference of the output voltage is considered (see Fig. 9). At time $t = 4\,\text{ms}$, the output voltage reference changes from $V_{o,\text{ref}} = 45\,\text{V}$ to $V_{o,\text{ref}} = 55\,\text{V}$. The controller instantaneously increases the current (Figs. 9(b) and 9(c)) to quickly ramp up the output voltage (Fig. 9(a)). The controller exhibits an excellent behavior during the transient, reaching the new output voltage in about $t \approx 6\,\text{ms}$, without any overshoot.

However, when a PI controller is used (Fig. 10) the transient lasts longer. The current does not significantly increase to fast charge the capacitor to the new desired level (Figs. 10(b) and 10(c)); the output voltage reaches its new demanded value in about $t \approx 40\,\text{ms}$.

Load Step Change

The last case examined is that of a step-down change in the load resistance, see Fig. 11. At time $t = 3\,\text{ms}$ the load decreases from $R = 75\,\Omega$ to $R = 50\,\Omega$. The proposed MPC strategy manages to adjust to the non-nominal operating conditions; the system reaches the new operating point very quickly in about $t \approx 1\,\text{ms}$ (Fig. 11(a)). On the other hand, when a PI controller is employed (Fig. 12), the converter settles at the new operating point in about $t \approx 65\,\text{ms}$ (Fig. 12(a)).

Conclusions

This paper proposes a model predictive current controller for the interleaved dc-dc boost converter with coupled inductors, which shows very fast dynamic responses. An objective function is formulated using model predictive control (MPC), while hard constraints for the switchings and soft constraints for the input current (sum of the inductor currents) are employed in order to achieve the control objectives. The introduced strategy achieves robustness for the entire operating range. Furthermore, the controller achieves equal current distribution, and exploits the benefits of both continuous (CCM) and discontinuous (DCM) conduction modes. These advantages overshadow the inherent drawbacks of the method, such as the computational complexity and the variable switching frequency. Nonetheless, the implementation of MPC as a current controller enables the use of a relatively short prediction horizon, allowing a decrease in the computational burden. Simulation results demonstrate the high performance of the proposed methodology.

References

[1] N. Mohan, T. M. Undeland, and W. P. Robbins, *Power Electronics: Converters, Applications and Design*, 3rd ed. Hoboken, NJ: Wiley, 2003.

[2] P.-W. Lee, Y.-S. Lee, D. Cheng, and X.-C. Liu, "Steady-state analysis of an interleaved boost converter with coupled inductors," *IEEE Trans. Ind. Electron.*, vol. 47, no. 4, pp. 787–795, Aug. 2000.

[3] J. M. Maciejowski, *Predictive Control with Constraints*. Englewood Cliffs, NJ: Prentice-Hall, 2002.

[4] D. Q. Mayne, J. B. Rawlings, C. V. Rao, and P. O. M. Scokaert, "Constrained model predictive control: Stability and optimality," *Automatica*, vol. 36, no. 6, pp. 789–814, Jun. 2000.

[5] T. Geyer, G. Papafotiou, R. Frasca, and M. Morari, "Constrained optimal control of the step-down dc-dc converter," *IEEE Trans. Power Electron.*, vol. 23, no. 5, pp. 2454–2464, Sep. 2008.

[6] T. Geyer, G. Papafotiou, and M. Morari, "Hybrid model predictive control of the step-down dc-dc converter," *IEEE Trans. Contr. Syst. Technol.*, vol. 16, no. 6, pp. 1112–1124, Nov. 2008.

[7] A. G. Beccuti, G. Papafotiou, R. Frasca, and M. Morari, "Explicit hybrid model predictive control of the dc-dc boost converter," in *Proc. IEEE Power Electron. Spec. Conf.*, Orlando, FL, Jun. 2007, pp. 2503–2509.

[8] P. Karamanakos, G. Papafotiou, and S. Manias, "Model predictive control strategies for dc-dc boost voltage conversion," in *Proc. Eur. Power Electron. Conf.*, Birmingham, UK, Aug./Sep. 2011, pp. 1–9.

[9] P. Karamanakos, G. Papafotiou, and S. N. Manias, "Model predictive control of the interleaved dc-dc boost converter," in *Proc. Int. Conf. Syst. Theory, Control and Comp.*, Sinaia, Romania, Oct. 2011, pp. 1–6.

[10] P. Karamanakos, T. Geyer, and S. Manias, "Direct model predictive current control of dc-dc boost converters," in *Proc. Int. Power Electron. and Motion Control Conf. and Expo.*, Novi Sad, Serbia, Sep. 2012, pp. DS2c.11–1–DS2c.11–8.

[11] ——, "Direct voltage control of dc-dc boost converters using model predictive control based on enumeration," in *Proc. Int. Power Electron. and Motion Control Conf. and Expo.*, Novi Sad, Serbia, Sep. 2012, pp. DS2c.10–1–DS2c.10–8.

[12] A. Bemporad and M. Morari, "Control of systems integrating logic, dynamics and constraints," *Automatica*, vol. 35, no. 3, pp. 407–427, Mar. 1999.

[13] C. T. Chen, *Linear System Theory and Design*, 3rd ed. New York: Oxford Univ. Press, 1998.

[14] T. Geyer, G. Papafotiou, and M. Morari, "A hybrid model predictive control approach to the direct torque control problem of induction motors," *Int. J. of Robust Nonlinear Control*, vol. 17, pp. 1572–1589, May 2007.